Mooring Design Using Wave-State Estimate from the Southern Ocean

E. W. SCHULZ

Centre for Australian Weather and Climate Research, and Australian Bureau of Meteorology, Melbourne, Victoria, Australia

M. A. GROSENBAUGH

Woods Hole Oceanographic Institution, Woods Hole, Massachusetts

L. PENDER

Commonwealth Scientific Research Organisation, Hobart, Tasmania, Australia

D. J. M. GREENSLADE

Centre for Australian Weather and Climate Research, and Australian Bureau of Meteorology, Melbourne, Victoria, Australia

T. W. TRULL

Centre for Australian Weather and Climate Research, Commonwealth Scientific Research Organisation, University of Tasmania, and Antarctic Climate and Ecosystems Cooperative Research Centre, Hobart, Tasmania, Australia

(Manuscript received 18 November 2010, in final form 20 May 2011)

ABSTRACT

The Southern Ocean Flux Station was deployed near 47°S, 140°E. The extreme wind and wave conditions at this location require appropriate mooring design, which includes dynamic fatigue analysis and static analysis. An accurate estimate of the wave conditions was essential. A motion reference unit was deployed in a nearby test mooring for 6 months. The motion data provided estimates of significant wave height that agreed well with the Australian Bureau of Meteorology wave model, increasing confidence in the model performance in the Southern Ocean. The results of the dynamic fatigue analysis using three input wave datasets and implications for the mooring design are described. The design analysis predicts the fatigue life for critical mooring components and guided the final selection of links and chain shackles. The three input wave climatologies do not differ greatly, and this is reflected in minimal changes to mooring components for each of the fatigue analyses.

1. Introduction

The critical role of air–sea interaction in the coupled global climate system has been recognized for some time. This has been reflected in the increasing number of field experiments dedicated to observing and understanding the coupled system in recent decades, from the early Frontal Air–Sea Interaction Experiment (FASINEX; Weller 1991) in 1986 to the seminal Tropical Ocean Global Atmosphere Coupled Ocean–Atmosphere Response Experiment (TOGA COARE) in 1992–93 (Webster and Lukas 1992). A variety of platform technologies, typically including ships, aircraft, and moorings, were deployed in these field experiments for intensive observing periods spanning at most a few months. It was recognized that moored instrumented surface buoys, such as that depicted in Fig. 1 were necessary to obtain the long-term observations needed to study larger-scale phenomena. The task of operating an unattended mooring for extended periods of time in the open ocean is very challenging. The combined forces of wind, waves, and currents act to stress the mechanical structure and sensors, while biofouling, fish bite, and vandalism must also

Corresponding author address: E. W. Schulz, GPO Box 1289, Centre for Australian Weather and Climate Research, Bureau of Meteorology, Melbourne, VIC 3001 Australia.
E-mail: e.schulz@bom.gov.au

DOI: 10.1175/JTECH-D-10-05033.1

be countered. Mooring failure continues to be a common occurrence, although information on the circumstances of the failures is difficult to obtain. Extended mooring deployments were first attempted in the mid-1960s, with limited success achieved by the 1970s with 1-month deployments, such as the Mixed Layer Experiment (MILE; Davis et al. 1981a,b) and the Joint Air–Sea Interaction Study (JASIN; Pollard 1978). The Long Term Upper Ocean Study (LOTUS) Briscoe and Weller (1984) achieved a 2-yr time series using four consecutive 6-month mooring deployments from 1982 to 1984. TOGA COARE was the catalyst for the establishment of a permanent array of moorings in the tropical Pacific Ocean; the Tropical Atmosphere Ocean (TAO) project (McPhaden et al. 1998) provided long-term monitoring of the coupled tropical El Niño–Southern Oscillation. This was later extended westward as the Triangle Trans-Ocean Buoy Network (TRITON), into the tropical Indian Ocean via the Research Moored Array for African–Asian–Australian Monsoon Analysis and Prediction (RAMA; McPhaden et al. 2009), and eastward via the Prediction and Research Moored Array in the Tropical Atlantic (PIRATA; Servain et al. 1998) to complete the Global Tropical Moored Buoy Array (McPhaden et al. 2010). A number of isolated long-term mooring occupations commenced during the last decade at locations such as the eastern tropical Pacific [Stratus Deck Regions of the Eastern Pacific (STRATUS), East Pacific Investigation of Climate Processes in the Coupled Ocean-Atmosphere System (EPIC); see Raymond et al. (2004)], the northwest tropical Atlantic, the central Pacific [the Woods Hole Oceanographic Institution (WHOI) Hawaii Ocean Time-series (HOT) Site (WHOTS)], the North Atlantic Gulf Stream [Climate Variability and Predictability (CLIVAR) Mode Water Dynamics Experiment (CLIMODE); see Marshall et al. 2009], and the Kuroshio in the northwest Pacific [*Kuroshio* Extension Observatory (KEO) and Japanese *Kuroshio* Extension Observatory (JKEO); see Cronin et al. (2008)].

Typical mooring deployments now have durations of around 1 yr. Longevity has been achieved by advances in mooring design, materials, electronics, and instrumentation. Designs to minimize the impact of vandalism (McPhaden et al. 2010), drag from currents (Lawrence-Slavas et al. 2006), fish bite, and biofouling have all contributed to extending deployment length. Advances in technology have led to improvements in batteries, system power consumption, and data telemetry. Robust instrument design and instrument mounting strategies (e.g., Weller et al. 2008) have also improved observational capability. During the 1960s moorings were deployed in benign locations where currents were the dominant forcing and engineering design only needed to consider static tension. By the 1980s moorings were being deployed in rougher environments where wave forcing dominated and design needed to include cyclic fatigue (Trask 1995; Grosenbaugh 1995; Hamilton et al. 2003), as well as static loading.

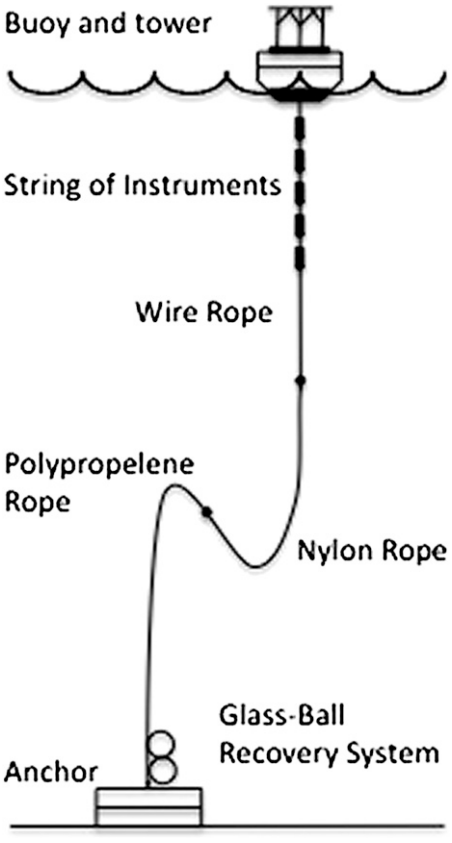

FIG. 1. Schematic of an inverse-catenary ''slack line'' oceanographic surface mooring consisting of surface float and tower, instruments strung along wire rope, a section of negatively buoyant nylon rope, a section of positively buoyant Polypropylene rope, a glass ball recovery system, and an anchor. The increased scope reduces mean tension from currents. Figure adapted from Grosenbaugh (1995).

Until now, there have been no in situ measurements of surface fluxes in the Southern Ocean. However, a large moored surface float—the Southern Ocean Flux Station (SOFS)—has been deployed as part of the Australian Integrated Marine Observing System (IMOS; see Meyers 2008; Hill 2010) Southern Ocean Times Series (SOTS; Fig. 2). To achieve this, the mooring had to be designed appropriately for the extreme wind, wave, and current environment in this region. The design process included dynamic fatigue analysis as well as static analysis. One of the inputs critical to achieving a realistic analysis was an accurate estimate of the wave conditions. There were no in situ estimates at such a remote location, and while satellite observations and models can provide

estimates of wave conditions, they do so with some uncertainty because of the lack of ground truthing. The design of SOFS will be refined in the future by examining how the mooring performed and the level of fatigue experienced during the deployment. In addition, this information can be used to evaluate the analysis technique.

The Australian Commonwealth Scientific Industrial Research Organization (CSIRO) developed a system based upon a commercial motion reference unit (MRU) that is capable of recording the motion of a moored surface float. This was deployed in a test mooring (Pulse) for 6 months in the Southern Ocean at 44°S, 146.5°E. The MRU data were postprocessed to yield estimates of significant wave height (H_s) and peak period (T_p) that were compared to the Australian Bureau of Meteorology (BOM) operational mesoscale wave model (MesoWAM; National Meteorological and Oceanographic Centre 2002). The results show remarkable agreement, with increasing confidence in MesoWAM performance in the Southern Ocean at the SOTS site and, as a corollary, indication that the MRU provides credible observations of the sea state.

In this paper, the dynamic fatigue analysis was performed for the SOFS mooring using three different input wave datasets, including the MesoWAM analysis at the SOTS site. In section 2, the dynamic fatigue analysis method is described. Section 3 describes the input wave datasets, including validations of MesoWAM in the region of interest. Results and implications for the mooring design are presented in section 4, and a summary is given in section 5.

2. The dynamic fatigue analysis method

Moorings deployed in high-wave environments are subject to cyclic loading in addition to current induced static loading, and thus fatigue failure. A design that can withstand the maximum forces of a single ''100-year return'' storm may fail due to repeated loading from a series of lesser storms. The magnitude of the forces that cause fatigue failure can be well below the ultimate strength of the mooring components. Thus, for moorings placed in high-wave environments where components can experience repeated oscillatory loading, it is critical to analyze moorings for fatigue failure.

The SOFS design is based on a dynamic fatigue analysis that includes a static, current-induced component, with the main focus here on the dynamic wave-driven part of the problem. The fatigue analysis follows from Grosenbaugh (1995) and is based on the Palmgren–Miner theory for cumulative damage. The load on a mooring component consists of an oscillatory dynamic tension superimposed on a mean tension. The analysis assumes that the mooring component loses a small fraction of life for each oscillatory cycle. The amount of loss depends primarily on the amplitude of the cycle, with a correction included for the mean. The total life lost is the sum over the total number of loading cycles. A mooring component will experience over 1 million cycles of loading during a year-long deployment.

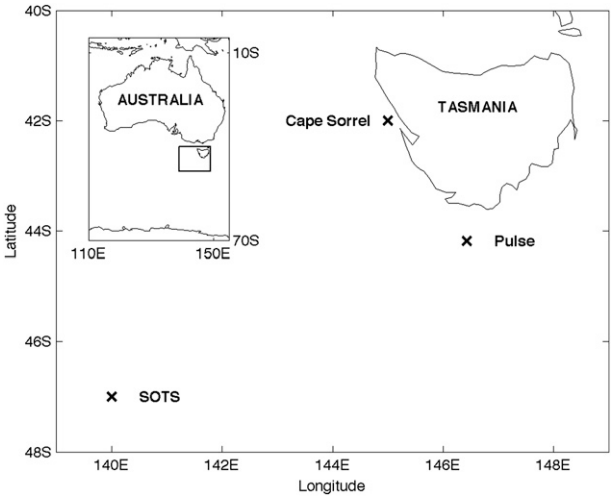

FIG. 2. Location of the Waverider buoy at Cape Sorrel, the Pulse test mooring, and the SOTS.

The loading history was derived by defining the environmental forcing in terms of a set of sea states and a mean current profile. A time series of H_s was analyzed to create a histogram of the loading history. Parameterizations of wind speed and T_p were computed as a function of H_s based on time series and added to the loading history. This simplification of the input to just a single variable was justified because the analysis is relatively insensitive to wind speed and T_p. The histogram provided the probability of occurrence of each sea state (from H_s) and associated wind speed and T_p. The loading history was input into a numerical model of mooring dynamics (Gobat and Grosenbaugh 2006), which was used to calculate the mooring tension. The fraction of damage to a mooring component resulting from all occurrences of a particular sea state over the deployment period was computed from the probability, number of cycles (from T_p), and magnitude of the oscillation (from H_s) (Grosenbaugh 1995). The analysis took into account the material properties of each mooring component that had been determined from laboratory cyclic-stress experiments (Trask and Weller 1995) where each component is cyclically stressed to destruction. The total fraction of damage was the sum of the damage over all sea states. For a mooring component to be acceptable, it had to lose less than 0.25 of

its life. For a 1-yr deployment, there would be a safety factor of greater than 4 (i.e., the mooring was designed so that the components could last more than 4 yr). The factor of 4 accounts for known bias in the Palmgren–Miner method for random loading, the effects of corrosion (Collins 1993), and unmodeled wear between adjacent components.

3. Wave datasets

In this analysis the probability of occurrence determines how many tension cycles are associated with each sea state. Wave observations are rare in the Southern Ocean, hence, we consider three different wave model estimates to determine the occurrences of sea states.

a. Datasets A and B

Dataset A is a 10-yr WAM (WAMDI Group 1988; Komen et al. 1994) hindcast time series of H_s, T_p, and wind speed for a Southern Ocean site at 55°S, 90°W near the southern tip of South America. At the time that the design analysis was performed, this was the only dataset that was available and easily accessible. This site is distant from the SOTS site but is expected to provide summary wave statistics that are broadly similar.

To make adjustments for the SOTS location, a value of 1.37 m was added to H_s in dataset A. This adjusted time series is dataset B. The 1.37-m value was based on Fleet Numerical Meteorology and Oceanography Center forecasts, which predict that a major 12-h storm with H_s greater than 9 m will occur at the SOTS site roughly every 2 weeks.

b. Dataset C

Dataset C is derived from the BOM's operational wave forecast system MesoWAM (National Meteorological and Oceanographic Centre 2002), which is a high-resolution (0.125° in latitude and longitude) nonassimilating regional version of the wave model (WAM; WAMDI Group 1988; Komen et al. 1994). Surface forcing is provided by the numerical weather prediction system and boundary conditions from a coarse-resolution data-assimilating WAM. Routine verification at a Waverider buoy located on the west coast of Tasmania at Cape Sorrel (42°S, 145°E; see Fig. 2) shows that H_s forecasts from MesoWAM typically have an rms error of less than 0.5 m and a positive bias of around 0.1 m at this location (National Meteorological and Oceanographic Centre 2009). Similar results are obtained for verifications of the global version of the model against satellite altimeter data (Durrant et al. 2009).

FIG. 3. The Pulse surface float.

1) THE MOTION REFERENCE UNIT AND PULSE TEST MOORING

A nearby mooring (Pulse) provided a further opportunity to verify MesoWAM in the region of interest. The Pulse test mooring was deployed at 44°11′S, 146°26′E (Fig. 2) for 6 months from 1 October 2008 to 9 April 2009, and carried an MRU, which measures wave heave spectra over the frequency range from 0.0195 to 5 Hz (corresponding to periods of 51.2–0.2 s) and can be used to estimate H_s, on the assumption that the Pulse buoy is a reasonable wave follower.

The Pulse mooring consists of a small surface float connected to a large damper/mass at 30-m depth via an elastic section (Pender et al. 2010; Trull et al. 2010). The surface float is effectively decoupled from the mooring and is a reasonable wave follower below wavelengths greater than a few meters because the buoy diameter is small (1 m; see Fig. 3) relative to the wavelength, and the buoy reserve buoyancy is much greater than the tether (bungee) restoring force at peak wave heights.

Pulse is equipped with an MRU, the low-cost and low–power consumption Microstrain 3DM-GX1 attitude sensor, configured to sample at 10 Hz for 10 min every 90 min. The MRU was configured to output three-axis relative accelerations and quaternions for the rotation of the relative accelerations to earth coordinates. Spectra are determined using Welch's method (Welch 1967) and 512-point fast Fourier transforms (FFTs). The log of spectral noise is a linear function of the log of frequency and can be regressed between very low and high frequencies where wave-induced motion is small. A similar filtering algorithm is reported by Earle et al. (1984). Figure 4 shows a comparison of the spectra derived in a laboratory test between the MRU system and the Waverider buoy with excellent agreement between the two systems. Here, H_s is

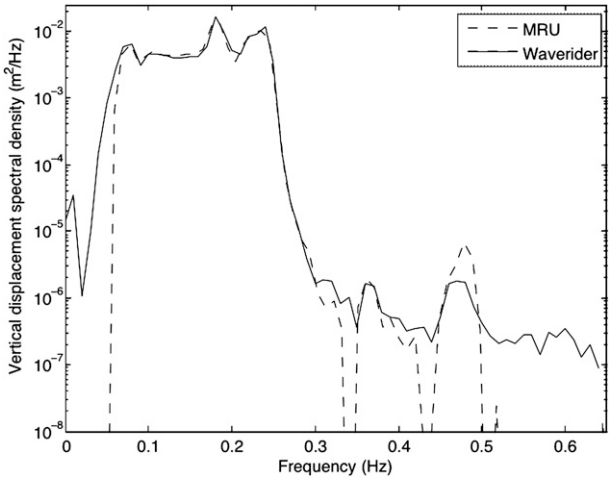

FIG. 4. Comparison of vertical displacement spectra determined from the MRU system (dashed) and a Waverider buoy (solid). The MRU system was mounted on top of the Waverider buoy in the calibration rig programmed to sweep between rotation periods of 5–15 s.

derived from the equation $4 \times \sqrt{\sum_3^{100} S_n}$, where S_n is the nth filtered vertical displacement spectral component. The summation is performed over waves with periods of between 0.5 and 17 s.

2) MRU–MESOWAM COMPARISON

Both H_s and T_p were extracted from the MesoWAM data at the nearest model grid location (44°7′S, 146°23′E) over the Pulse deployment time period. The comparison of H_s between MesoWAM and the MRU on Pulse (Fig. 5, top panel) indicates that we can have some confidence in both the sea-state estimates from the MRU and the wave field generated by MesoWAM at the Pulse site. The correlation is high at 0.87, with MesoWAM overestimating H_s marginally (by 0.05 m, or 4%) compared to the MRU and with a standard deviation 0.6 m. The comparison of T_p (Fig. 5, bottom panel) is a more difficult test, and MesoWAM appears to underestimate T_p (with a bias of −0.7 s, or 4%) compared to the MRU, with a correlation of ~0.5, although the discretization of the data makes the comparison challenging. The U.S. National Data Buoy Center developed a similar system to the MRU based on the same MicroStrain sensor. One-month comparisons with the Datawell Hippy 40 Mk II yielded mean (rms) differences in H_s of −0.02 (0.03) m and 0.13 (1) s for T_p (Teng et al. 2009). Results reported here have somewhat larger biases and standard deviations, which is not surprising given that the comparison is between in situ point measurement and model cell data.

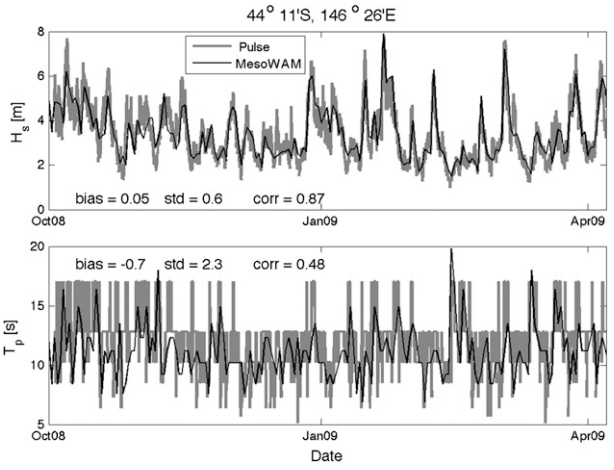

FIG. 5. (top) Significant wave height (H_S) and (bottom) T_p for the Pulse observations (thick gray) and MesoWAM analysis (thin black). Statistics (MesoWAM–Pulse) are also computed with the observations subsampled and averaged to match the model data time.

3) MESOWAM WAVES AT SOTS SITE

The Pulse test and SOTS sites are expected to have similar wind and wave conditions, because both are exposed to very long fetches to the west across the Southern Ocean and in deep water (>1000 m). The two locations are separated by 550 km, which is at the lower limit for synoptic-scale weather, so there is some justification in translating confidence in MesoWAM skill at the Pulse site to the SOTS site (Fig. 2). MesoWAM estimates of H_s and T_p at the SOTS site were extracted for the period from July 2002 to April 2009 (Fig. 6); this provides dataset C.

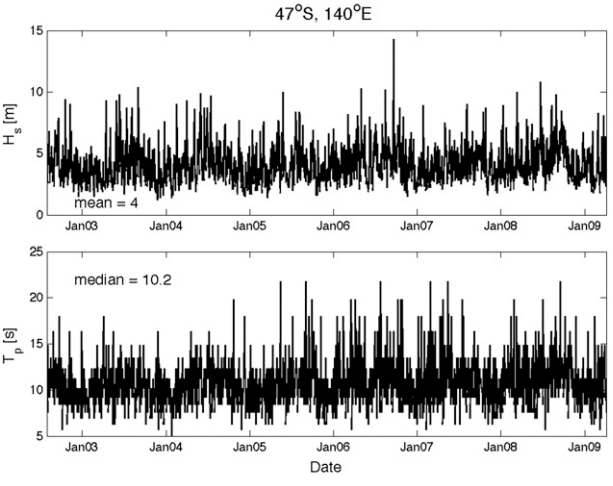

FIG. 6. (top) H_S and (bottom) T_p from MesoWAM at the SOTS site for the period Jul 2002 to Apr 2009.

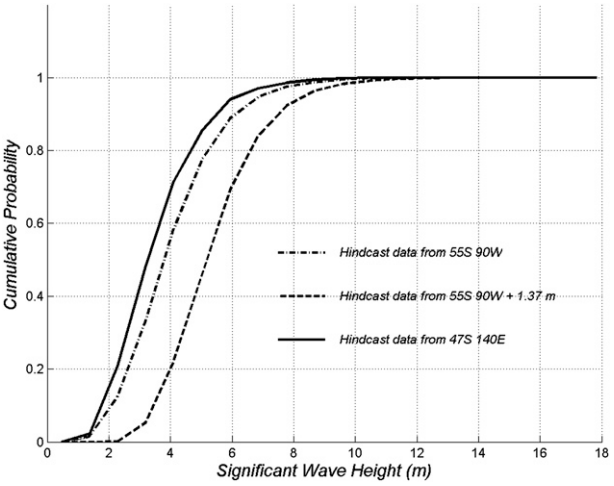

FIG. 7. Cumulative probability distribution for the three datasets.

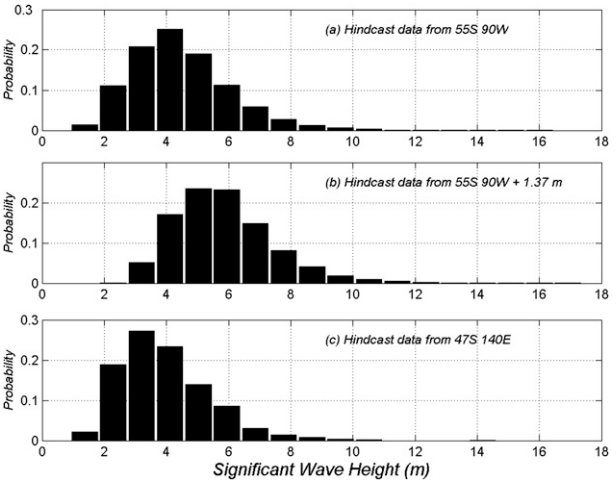

FIG. 8. The H_S percentage of occurrence based on (top) dataset A, (middle) dataset B with a 1.37-m positive bias, and (bottom) dataset C MesoWAM at SOTS site.

c. Sea-state characteristics

Figure 7 shows a comparison of the cumulative probability distribution for each of the three datasets, and Fig. 8 displays histograms of the percentage occurrence of H_s for each dataset. It can be seen from Fig. 7 that dataset C is the calmest and dataset B is the roughest. The adjustment of dataset A to dataset B can be seen to shift the histogram to the right (Fig. 8, top and middle panels). The shape of the histogram is altered slightly because the bin size is 0.9 m[1] compared to the shift of 1.37 m.

The histogram of dataset A is characterized by a peak of 25% in H_s occurrence in the 4.1-m bin. The histogram of dataset B (Fig. 8, middle panel) is identical to dataset A, except the x axis is shifted to the right by 1.37 m. This moves the most frequently occurring H_s to the 5- and 6-m bins. The histogram of dataset C (Fig. 8, bottom panel) is characterized by the most frequent (27%) with H_s occurring in the 3.2-m bin.

The H_s frequency distribution is tabulated (Table 1). The mooring design analysis also requires input of the mean 10-m wind (U_{10}) and T_p. These values are parameterized as a function of H_s for each bin based on linear best fits from dataset A, as $T_p = 0.87H_s + 4$ and $U_{10} = 1.34H_s + 5.25$.

4. Analysis with three wave datasets and design implications

The design elements for the upper portion of the SOFS mooring are displayed in Fig. 9. The subsurface mooring assembly consists of 8 m of 7/8-in. chain, 790 m of 7/16-in. and 900 m of 3/8-in. galvanized torque-balanced wire rope with an extruded jacket, 300-m wire-nylon splice, 2000 m of 7/8-in. eight-strand nylon, 1700 m of 1-in. eight-strand Colmega, glass sphere flotation, dual acoustic releases, and an anchor. Mooring scope is 1.35 with a design water depth of 4300 m. Significant instrument packages are two Aanderra Seagaurd RCM, weighing 10 kg in water (excluding the cage) at 30 and 200 m. End links and chain shackles are used for terminations to transition between chain, wire rope, and

TABLE 1. Frequency distribution of H_s for input datasets A, B, and C.

	Occurrence (%)				
H_s (m)	Dataset A	Dataset B	Dataset C	T_p (s)	U_{10} (m s^{-1})
1.4	1.47	0.00	2.17	5.2	7.1
2.3	11.07	0.12	18.83	6.0	8.3
3.2	20.86	5.22	27.30	6.8	9.6
4.1	25.13	17.10	23.29	7.6	10.8
5.0	19.01	23.57	13.92	8.4	12.0
6.0	11.33	23.28	8.51	9.2	13.2
6.9	5.82	14.83	3.07	10.0	14.5
7.8	2.80	8.16	1.47	10.8	15.7
8.7	1.30	4.14	0.82	11.6	16.9
9.6	0.72	1.83	0.41	12.3	18.2
10.5	0.33	0.96	0.16	13.1	19.4
11.4	0.09	0.51	0.00	13.9	20.6
12.4	0.03	0.18	0.00	14.7	21.8
13.3	0.01	0.06	0.00	15.5	23.1
14.2	0.01	0.00	0.04	16.3	24.3
15.1	0.01	0.01	0.00	17.1	25.5
16.0	0.01	0.01	0.00	17.9	26.8
17.0	0.00	0.02	0.00	18.7	28.0

[1] A bin width of 0.9 m was selected by dividing the range of H_s values (1.4–17 m) in dataset B into an arbitrary 17 bins.

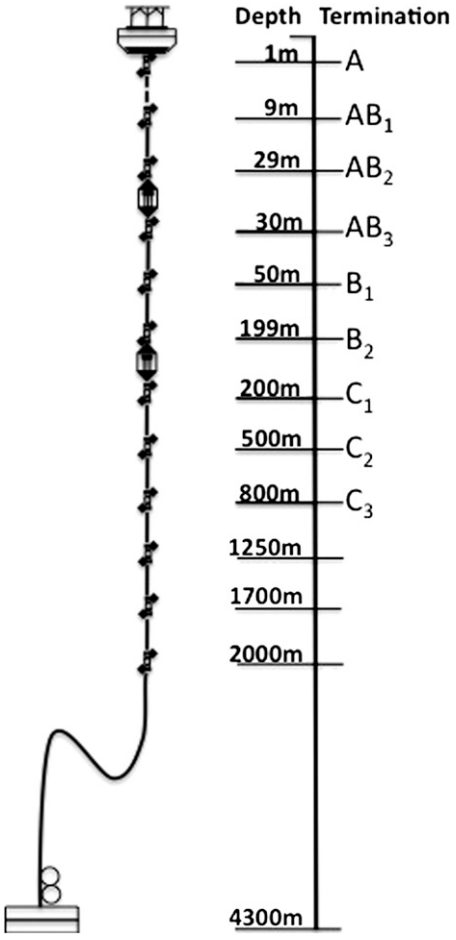

FIG. 9. The SOFS mooring design. Design elements are terminations (end link and chain shackles), chain, wire rope, instrument cages, wire-to-rope termination, and synthetic line. The top section consists of 8 m of 7/8-in. chain, then 7/16-in. wire rope down to 800 m, 3/8-in. wire rope down to 2000 m, a wire-to-rope termination at 2000 m, and then 2000 m 7/8-in. nylon and 1700 m 1-in. Colmega. Scope is 1.35. The termination depths are indicated. Terminations below 800 m are not labeled as they are subject to negligible fatigue. Diagram is not to scale.

instrument cages. A current profile was derived from 2 yr of observations from a subsurface mooring at 50.7°S, 143.25°E in the Antarctic Circumpolar Current. The design can survive a current profile of 1, 0.37, and 0.12 m s^{-1}, at depths of 0 (surface), 1000, and 3200 m, respectively, which yields maximum mean tensions of around 900 kg just under the buoy. Results are presented for the most critical components and exclude other components such as wire-rope sockets and synthetic terminations. The results of the analysis for the end links and chain shackles are given in Tables 2–5. Letters and subscript numbers are used to specify the termination. Termination "A" is located at the very top of the mooring just below the buoy. It experiences the highest tensions.

TABLE 2. Analysis of 1-in. Crosby weldless end link. Forged carbon steel, quenched and tempered, and hot dip galvanized.

		Expected life (years)		
Terminal	Depth (m)	A	B	C
	1	8.1	7.3	8.7
AB_1	9	9.2	8.4	9.7
AB_2	29	9.6	8.8	10.1
AB_3	30	10.9	10.1	11.4

The subsequent terminations in the table are located in order of depth; each experiences less and less tension because the load is primarily due to the weight and acceleration of the mooring components below (i.e., deeper than) the termination location. Note that all of the terminations located below C_3 (800 m) in the mooring line have no fatigue issues. Tables 2 and 3 give the expected life of 7/8- and 1-in. Crosby end links for each of the three sea-state probability functions in Fig. 8. The mean tension plays a very minor role in determining the expected life of the terminations. Tables 4 and 5 provide the expected life for 7/8- and 3/4-in. chain shackles. The inverse of these values is the fraction of life lost for a 1-yr deployment. Bold numbers in Tables 3 and 5 indicate parts that are not acceptable for a 1-yr deployment because they are calculated to lose more than one-fourth of their life during a 1-yr deployment. In these cases 1-in. end links (Table 2) and/or 7/8-in. chain shackles (Table 4) were used.

The expected life decreases when using dataset B and increases when using dataset C, consistent with the cumulative probability distributions of the three input datasets (Fig. 7). The only significant difference when using any of the three input datasets is with regards to the 7/8-in. end link at termination AB_3, which is the

TABLE 3. Analysis of 7/8-in. Crosby weldless end link. Forged carbon steel, quenched and tempered, and hot dip galvanized. Boldface indicates parts that are not acceptable for a 1-yr deployment because they are calculated to lose more than one-fourth of their life during a 1-yr deployment.

		Expected life (years)		
Terminal	Depth (m)	A	B	C
A	1	**3.2**	**2.9**	**3.4**
AB_1	9	**3.6**	**3.3**	**3.8**
AB_2	29	**3.8**	**3.5**	**4.0**
AB_3	30	4.3	**4.0**	4.5
B_1	50	5.4	5.0	5.6
B_2	199	6.4	6.1	6.6
C_1	200	22.5	21.7	23.2
C_2	500	98.8	94.6	>100
C_3	800	>100	>100	>100

TABLE 4. Analysis of 7/8-in. chain shackle. Forged, shot peened, and painted.

Terminal	Depth (m)	Expected life (years)		
		A	B	C
A	1	4.5	4.1	4.8
AB_1	9	5.1	4.6	5.4
AB_2	29	5.3	4.9	5.6
AB_3	30	6.0	5.6	6.3
B_1	50	7.5	7.1	7.9
B_2	199	9.0	8.6	9.3

fourth termination below the buoy at a depth of about 30 m and at the top of a 20-m length of wire rope. Datasets A and C predict 4.3 and 4.5 yr of life, respectively. Dataset 2 predicts only 4.0 yr of life, which is just below the acceptable criteria. These values are consistent with the probability values (Table 1) for large storms ($H_s >$ 12 m), which cause most of the fatigue damage. The fatigue analysis results using dataset B are used in the final mooring design because this represents the most extreme set of wave conditions from the three datasets, and is therefore the more conservative approach. The end links and chain shackles selected for each terminal are displayed in Table 6.

Termination hardware such as end links and shackles are very susceptible to fatigue. However, it is the sum of the mass of the chain, wire rope, instruments, and cages hanging below the termination that determines the stress and therefore dictates the size of the mooring components. The addition of even relatively small masses can significantly increase the peak loading as the mass accelerates under large wave amplitude forcing. During the SOFS analysis, the removal of a 30-kg instrument package at 50-m depth and the reduction of the length of 7/8-in. chain in the top of the mooring halved the peak loading and increased the mooring years of life 13-fold (from just 150 days to 5.5 yr). In addition, the use of larger shackles may dictate the use of larger chain to ensure even contact and minimize point loading and wear between shackle and chain. Larger chain in turn increases the overall loading on the mooring.

5. Summary

The Southern Ocean provides a challenging environment for the deployment of long-term surface moorings. SOFS is the first successful long-term large surface expression mooring deployment in the Southern Ocean other than Deep-Ocean Assessment and Reporting of Tsunamis (DART) buoy tsunameters in the Tasman Sea near 47°S, 161°E. The consistently large waves and high winds provide strong surface forcing, which in turn generates significant fatigue on mooring components, such as shackles and links. Hence, it is essential to recognize fatigue analysis in the mooring design and input accurate surface forcing.

TABLE 5. Analysis of 3/4-in. chain shackle. Forged, shot peened, and painted. Boldface indicates parts that are not acceptable for a 1-yr deployment because they are calculated to lose more than one-fourth of their life during a 1-yr deployment.

Terminal	Depth (m)	Expected life (years)		
		A	B	C
A	1	**1.3**	**1.2**	**1.4**
AB_1	9	**1.5**	**1.4**	**1.6**
AB_2	29	**1.6**	**1.4**	**1.7**
AB_3	30	**1.8**	**1.6**	**1.9**
B_1	50	**2.2**	**2.1**	**2.3**
B_2	199	**2.6**	**2.5**	**2.7**
C_1	200	9.2	8.9	9.5
C_2	500	40.5	38.7	41.8
C_3	800	>100	>100	>100

A relatively small and inexpensive motion reference unit was trialed on a test mooring (Pulse). The MRU-derived estimates of H_s exhibited remarkable agreement with MesoWAM, leading to increased confidence in the ability of MesoWAM at the SOTS site. Two other wave climatology datasets were obtained from a wave model hindcast near the southern tip of South America.

The SOFS mooring design was evaluated for static loading from currents and dynamic fatigue effects on shackles and links using the three wave climatology datasets as input. It was found that the mooring design is relatively insensitive to variations between the roughest and calmest input datasets with differences of around 2.3 m in median H_s. The analysis indicates that the lighter 7/8-in. end links and 3/4-in. chain shackles do not meet the fatigue life requirements at terminations shallower than 29 and 199 m, respectively. A conservative

TABLE 6. SOFS mooring end link and shackle selection and expected life based on fatigue analysis with dataset A as input.

Terminal	Depth (m)	End link (1 in.)	End link (7/8 in.)	Chain shackle (7/8 in.)	Chain shackle (3/4 in.)
A	1	7.3		4.1	
AB_1	9	8.4		4.6	
AB_2	29	8.8		4.9	
AB_3	30	10.1		5.6	
B_1	50		5.0	7.1	
B_2	199		6.1	8.6	
C_1	200		21.7		8.9
C_2	500		94.6		38.7
C_3	800		>100		>100

approach is taken here and the most extreme of the three analyses is used in the final mooring design.

Acknowledgments. The Pulse and SOFS moorings are platforms contributing to the Southern Ocean Time Series (SOTS) Facility, a component of the Australian Integrated Marine Observing System (IMOS). From 2010 onward these moorings are part of the IMOS Australian Bluewater Observing System Facility. The Pulse mooring design effort was initiated by Tom Trull under the auspices of the Antarctic Climate and Ecosystem Cooperative Research Centre in 2003. Since 2006 it has been part of IMOS. Many years of logistic support for these deployments have been provided by the Australian Marine National Facility and the Australian Antarctic Sciences program (Award 1156). IMOS is funded through the Federal Government's National Collaborative Research Infrastructure Strategy and the Super Science Initiative.

REFERENCES

Briscoe, M. G., and R. A. Weller, 1984: Preliminary results from the Long-Term Upper Ocean Study (LOTUS). *Dyn. Atmos. Oceans,* **8,** 243–265.

Collins, J. A., 1993: *Failure of Materials in Mechanical Design*. John Wiley and Sons, 654 pp.

Cronin, M. F., C. Meinig, C. L. Sabine, H. Ichikawa, and H. Tomita, 2008: Surface mooring network in the Kuroshio Extension. *IEEE Syst. J.,* **2,** 424.

Davis, R. E., R. deSzoeke, D. Halpern, and P. Niiler, 1981a: Variability and dynamics of the upper ocean during MILE. Part I: The heat and momentum balances. *Deep-Sea Res.,* **28A,** 1427–1451.

——, ——, and P. Niiler, 1981b: Variability and dynamics of the upper ocean during MILE. Part II: Modelling the mixed layer response. *Deep-Sea Res.,* **28A,** 1453–1475.

Durrant, T. H., D. J. M. Greenslade, and G. R. Warren, 2009: Assessing upgrades to the Bureau of Meteorology's wave forecasting system using satellite altimeter data. CAWCR Tech. Rep. 12, Bureau of Meteorology Australia, 30 pp. [Available online at http://www.cawcr.gov.au/publications/technicalreports/CTR_012.pdf.]

Earle, M. D., K. E. Steele, and Y. H. L. Hsu, 1984: Wave spectra corrections for measurements with hull-fixed accelerometers. *Proc. Oceans'84*, Washington, DC, IEEE, 725–730.

Gobat, J. I., and M. A. Grosenbaugh, 2006: Time-domain numerical simulation of ocean cable structures. *Ocean Eng.,* **33,** 1373–1400.

Grosenbaugh, M. A., 1995: Designing oceanographic surface moorings to withstand fatigue. *J. Atmos. Oceanic Technol.,* **12,** 1101–1110.

Hamilton, A., M. Chaffey, E. Mellinger, J. Erickson, and L. McBride, 2003: Dynamic modeling and actual performance of the MOOS test mooring. MTS/IEEE Oceans Conf., San Diego, CA, IEEE, 2574–2581.

Hill, K., 2010: The Australian Integrated Marine Observing System (IMOS). *Meteor. Technol. Int.,* **1,** 114–118.

Komen, G. J., L. Cavaleri, M. Donelan, K. Hasselmann, S. Hasselmann, and P. A. E. M. Janssen, 1994: *Dynamic Modelling of Ocean Waves*. Cambridge University Press, 532 pp.

Lawrence-Slavas, N., C. Meinig, and H. Milburn, 2006: KEO mooring engineering analysis. NOAA Tech. Memo. OAR PMEL-130, 34 pp. [Available online at http://www.pmel.noaa.gov/pubs/PDF/lawr2930/lawr2930.pdf.]

Marshall, J. A., and Coauthors, 2009: The CLIMODE field campaign observing the cycle of convection and restratification over the Gulf Stream. *Bull. Amer. Meteor. Soc.,* **90,** 1337–1350.

McPhaden, M. J., and Coauthors, 1998: The Tropical Ocean-Global Atmosphere (TOGA) observing system: A decade of progress. *J. Geophys. Res.,* **103,** 14 169–14 240.

——, and Coauthors, 2009: RAMA: The Research Moored Array for African–Asian–Australian Monsoon Analysis and Prediction. *Bull. Amer. Meteor. Soc.,* **90,** 459–480.

——, and Coauthors, 2010: The global tropical moored buoy array. Proceedings of OceanObs'09: Sustained Ocean Observations and Information for Society, Vol. 2, ESA Publication WPP-306, Venice, Italy, ESA. [Available online at https://abstracts.congrex.com/scripts/jmevent/abstracts/FCXNL-09A02a-1748989-1-McPhaden_Oceanobs09.pdf.]

Meyers, G., 2008: The Australian Integrated Marine Observing System. *J. Ocean Technol.,* **3,** 80–81.

National Meteorological and Oceanographic Centre, 2002: Changes to the operational sea state forecast system. NMOC Analysis and Prediction Operations Bulletin 55, Bureau of Meteorology, 5 pp. [Available online at http://www.bom.gov.au/australia/charts/bulletins/opsbul55.pdf.]

——, 2009: Quarterly summary of operational performance, October-December 2009. Bureau of Meteorology, 71 pp.

Pender, L., T. W. Trull, D. Mclaughlan, and T. Lynch, 2010: Pulse—A mooring for mixed layer measurements in the open ocean and extreme weather. *OCEANS 2010,* Sydney, NSW, Australia, Paper 100114-070, doi:10.1109/OCEANSSYD.2010.5603604.

Pollard, R. T., 1978: The Joint Air–Sea Interaction Experiment—JASIN. *Bull. Amer. Meteor. Soc.,* **59,** 1310–1318.

Raymond, D. J., S. K. Esbensen, M. Gregg, and C. S. Bretherton, 2004: EPIC2001 and the coupled ocean–atmosphere system of the tropical east Pacific. *Bull. Amer. Meteor. Soc.,* **85,** 1341–1354.

Servain, J., A. Busalacchi, M. J. McPhaden, A. D. Moura, G. Reverdin, M. Vianna, and S. Zebiak, 1998: A Pilot Research Moored Array in the Tropical Atlantic (PIRATA). *Bull. Amer. Meteor. Soc.,* **79,** 2019–2031.

Teng, C.-C., R. Bouchard, R. Riley, T. Mettlach, R. Dinoso, and J. Chaffin, 2009: NDBC's digital directional wave module. NDBC Rep. 0-933957-38-1, 8 pp. [Available online at http://dodreports.com/pdf/ada527208.pdf.]

Trask, R. P., 1995: Mooring hardware fatigue tests for the Arabian Sea surface mooring. Woods Hole Oceanographic Institution Upper Ocean Process Group Tech. Note, 2 pp.

——, and R. A. Weller, 1995: Cyclic fatigue testing of surface mooring hardware for the Arabian Sea mixed layer dynamics experiment. Woods Hole Oceanographic Institution Tech. Rep. WHOI-95-16, 62 pp. [Available online at https://darchive.mblwhoilibrary.org/bitstream/handle/1912/518/WHOI-95-16.pdf?sequence=1.]

Trull, T. W., E. W. Schulz, S. G. Bray, L. Pender, D. McLaughlan, and B. Tilbrook, 2010: The Australian Integrated Marine Observing System Southern Ocean Time Series facility. *OCEANS 2010,*

Sydney, NSW, Australia, IEEE, Paper 100114-043, doi:10.1109/OCEANSSYD.2010.5603514 .

WAMDI Group, 1988: The WAM model—A third generation wave prediction model. *J. Phys. Oceanogr.,* **18,** 1775–1810.

Webster, P. J., and R. Lukas, 1992: TOGA COARE: The Coupled Ocean–Atmosphere Response Experiment. *Bull. Amer. Meteor. Soc.,* **73,** 1377–1416.

Welch, P. D., 1967: The use of fast Fourier transform for the estimation of power spectra: A method based on time averaging over short, modified periodograms. *IEEE Trans. Audio Electroacoust.,* **AU-15,** 70–73.

Weller, R. A., 1991: Overview of the Frontal Air-Sea Interaction Experiment (FASINEX): A study of air–sea interaction in a region of strong oceanic gradients. *J. Geophys. Res.,* **96,** 8501–8516.

——, E. F. Bradley, J. B. Edson, C. W. Fairall, I. Brooks, M. J. Yelland, and R. W. Pascal, 2008: Sensors for physical fluxes at the sea surface: Energy, heat, water, salt. *Ocean Sci.,* **4,** 247–263.